SCIENTIFIC REPORTS

OPEN

SUBJECT AREAS:
ELECTRONIC DEVICES
ORGANIC-INORGANIC NANOSTRUCTURES
BATTERIES
ELECTRICAL AND ELECTRONIC ENGINEERING

Received
1 May 2013

Accepted
10 July 2013

Published
25 July 2013

Correspondence and requests for materials should be addressed to Y.H.G. (gaoyihua@hust.edu.cn) or N.S.L. (nishuang_liu@foxmail.com)

* These authors contributed equally to this work.

Solid-State High Performance Flexible Supercapacitors Based on Polypyrrole-MnO_2-Carbon Fiber Hybrid Structure

Jiayou Tao[1,2]*, Nishuang Liu[1], Wenzhen Ma[1]*, Longwei Ding[1], Luying Li[1], Jun Su[1] & Yihua Gao[1]

[1]Center for Nanoscale Characterization and Devices (CNCD), Wuhan National Laboratory for Optoelectronics (WNLO)-School of Physics, Huazhong University of Science and Technology (HUST), Luoyu Road 1037, Wuhan 430074, P. R. China, [2]School of Physics and Electronics, Hunan Institute of Science and Technology, Yueyang 414006, P. R. China.

A solid-state flexible supercapacitor (SC) based on organic-inorganic composite structure was fabricated through an "in situ growth for conductive wrapping" and an electrode material of polypyrrole (PPy)-MnO_2 nanoflakes-carbon fiber (CF) hybrid structure was obtained. The conductive organic material of PPy greatly improved the electrochemical performance of the device. With a high specific capacitance of 69.3 F cm^{-3} at a discharge current density of 0.1 A cm^{-3} and an energy density of 6.16 × 10^{-3} Wh cm^{-3} at a power density of 0.04 W cm^{-3}, the device can drive a commercial liquid crystal display (LCD) after being charged. The organic-inorganic composite active materials have enormous potential in energy management and the "in situ growth for conductive wrapping" method might be generalized to open up new strategies for designing next-generation energy storage devices.

Owing to the rapid development of portable personal electronics, flexible electronics has attracted intense interests. Much effort has been dedicated in varied fields and great progress has been made to fabricate flexible devices, such as artificial electronic skin, roll-up displays and distributed sensors[1–4]. In order to realize fully flexible devices, all of these electronics require flexible, lightweight and high efficient energy storage units. Conventional energy storage devices, such as batteries, have limitations such as inflexible, relative low power and long charging time[5]. Supercapacitors (SCs), also known as electrochemical capacitors, in which electrical energy is mainly stored by fast and reversible redox reactions or phase changes on the surface or subsurface of electrodes[6–9], exhibit a promising set of features such as high power density, fast rates of charge-discharge, good cycle stability and safe operation[10,11]. In comparison with the SCs using liquid electrolyte, all solid-state SCs have certain advantages such as good flexibility, high safety and lightweight, which are in demand of flexible and portable devices[12–14].

Due to their high specific capacitance than carbon materials, transition metal oxides have been extensively studied in the past decades[15–21]. MnO_2, compared to the other transition metal oxides, is the most thoroughly investigated for pseudocapacitors on the basis of its high theoretical specific capacitance of 1370 F g^{-1} [22], relatively low cost and environmentally benign nature[23–25]. Being limited by its poor electrical conductivity, the theoretical specific capacitance of MnO_2 has rarely been achieved in experiment[22]. Considerable research efforts have been dedicated to improve the electrical conductivity of the active electrode materials and many materials have been fabricated on MnO_2, such as metal nanostructure[26], carbon nanotubes[27–30], graphene[24,31], or conductive organic matter[32–34]. The capacitance and conductivity of the hybrid structure based on MnO_2 can be improved more by conductive polymers according to the investigations[35–37], such as PPy, polyaniline and polythiophene, which have high electrical conductivity and high specific capacitance, and are easy to be polymerized and hold particular promise for potential large-scale energy storage systems. Even so, their improvement is not significant on the capacitance of MnO_2 and the reason is not clear. On the other hand, to meet the need of the flexibility of SCs, the flexibility of the current collector of SCs should be taken into account. CF is such a kind of materials with high flexibility as a current collector, and other advantages, such as high knittability, good conductivity. Therefore, CFs were applied in previous researches of SCs[38].

Herein, we developed an "in situ growth for conductive wrapping" method to rationally design an all solid-state SC based on PPy-MnO_2 nanoflakes-CF composites, which exhibited high flexible, high electrochemical performances. CF acted as the current collector, and MnO_2 nanoflakes were deposited through a electrodeposition process[37]. A thin layer of PPy wrapped around MnO_2 nanoflakes uniformly by "in situ growth" method which was different from the "dip-coating" process, not only provided an additional electron transport path besides CFs underneath MnO_2 nanoflakes but also actively participates in the charge storage process of electric double layer capacitance or pseudo-capacitance[34]. In addition, PPy can prevent MnO_2 nanoflakes from corrosion in acidic electrolyte, which ensure the full release of the electrochemical performances of MnO_2 nanoflakes in the whole device. Electrochemical and mechanical measurements indicated that the as-fabricated device showed a high specific capacitance of 69.3 F cm^{-3} at a discharge current density of 0.1 A cm^{-3} with a total capacitance of ~0.35 mF (Eq. 1 in SI), which were much higher than those values reported in literatures[37,39,40], and a high energy density of 6.16×10^{-3} Wh cm^{-3} at a power density of 0.04 W cm^{-3}. Furthermore, when it was rolled up, the electrochemical performance of the SC only had a slight fluctuation of about 0.24%.

Results

Fabrication of PPy-MnO_2-CF electrodes and the solid-state SC. The process of fabricating the solid-state SC consisted of four steps, as illustrated in Figure 1. A bunch of commercially available CFs (diameters 6.5–8.5 μm) was cut to shorter length (about 3 cm), then the fibers were cleaned by acetone, alcohol and deionized water with ultrasonic several cycles (Figure 1a). After drying completely in a vacuum oven, a CF was fixed on a teflon substrate and connected to an electrode. The next step was to electrodeposit MnO_2 on the CF (Figure 1b). MnO_2 nanoflakes have large specific surface area, which can enhance the electrochemical performances of the device significantly. In order to seek for the dependence of SC performance on MnO_2 deposition time, the deposition time of MnO_2 on CFs was different, ranging from 1 to 45 min. For the sake of enhancing the conductivity of MnO_2 nanoflakes, a layer of PPy was wrapped on the MnO_2-CFs (Figure 1c). Similar to the preparation of the MnO_2-CF, a constant voltage of 0.8 V was used during the deposition process of PPy and the deposition time was from 0.5 to 3 min. The last step was to incorporate a SC, as illustrated in figure 1d. A piece of common preservative film was laid out as the substrate. Two PPy-MnO_2-CFs were fixed on the film and assembled into a SC by sandwiching a PVA/H_3PO_4 membrane as the separator and the electrolyte between the two electrodes. When the device was charged completely, it could power a commercial LCD (Figure 1d).

Characterization of as-prepared PPy-MnO_2-carbon composites. Scanning electron microscopy (SEM) images of the electrodes showed that MnO_2 nanoflakes were uniformly deposited on the CFs (Figure 2a, b). MnO_2 nanoflakes have large specific surface area that can enhance electrochemical performances of the as fabricated SCs. With the increasing of the electrodeposition time, MnO_2 nanoflakes became larger and thicker (Supporting Figure S1). However, only the surface layer of MnO_2 could take the oxidation-reduction reaction[9], too much loading of MnO_2 might decrease the specific surface area and lower the conductivity of the electrodes. We found that the surface of CFs could be fully covered by MnO_2 nanoflakes after 15 min of electrodeposition (Figure 1b). As to solid-state SCs, the PVA/H_3PO_4 gel electrolyte was commonly used in fabricating process. We found that the flake-like MnO_2 nanomaterials was corroded easily by H_3PO_4 due to its larger specific surface area (Figure 3b). The nanostructure of MnO_2 was highly porous as revealed by transmission electron microscopy (TEM) images (Figure 2d, Supporting Figure S2), which was good for exchanging and transport of charges. The deposited MnO_2 are polycrystalline as demonstrated by a high resolution transmission electron microscopy (HRTEM) image together with selected area electron diffraction (SAED) pattern (Figure 2e and inset). It was further confirmed that the polycrystalline MnO_2 nanoflakes belong to ε-MnO_2 phase by X-ray diffraction (XRD) (Figure 2f). In order to improve the electrical conductivity of MnO_2-based electrodes and prevent corrosion for optimized electrochemical performance, PPy was electro-polymerized and wrapped on the MnO_2 nanoflakes (Figure 2c). The optimized deposition time of PPy was about

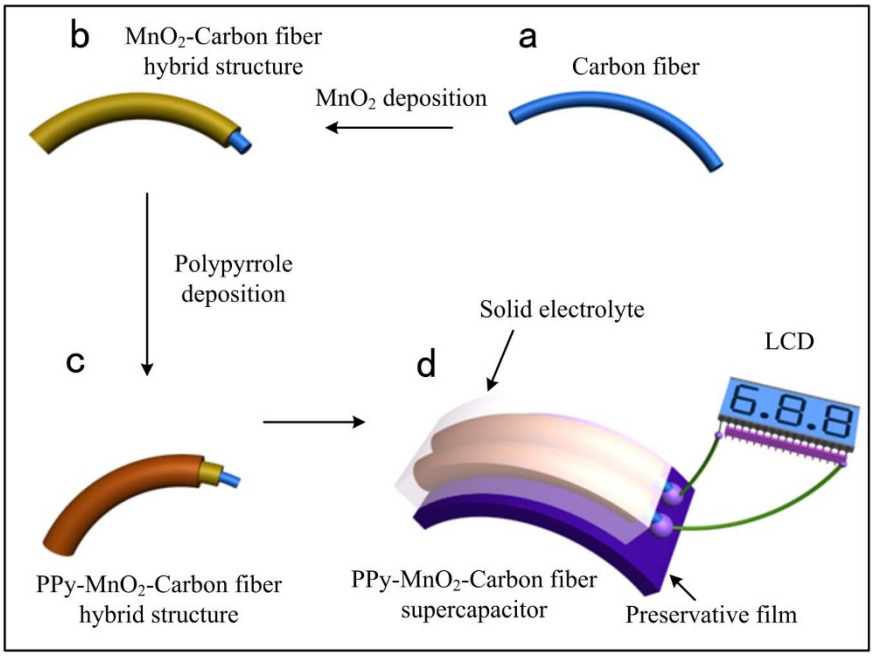

Figure 1 | Fabrication process of PPy-MnO_2-CF SCs. (a,b) A CF was cleaned and cut to shorter length; then MnO_2 nanoflakes were coated onto the CF by electrodepositon method; (c) PPy was electrodeposited onto the MnO_2-CF; (d) Two PPy-MnO_2-CFs were assembled on a piece of preservative film to form a PPy-MnO_2-CF SC.

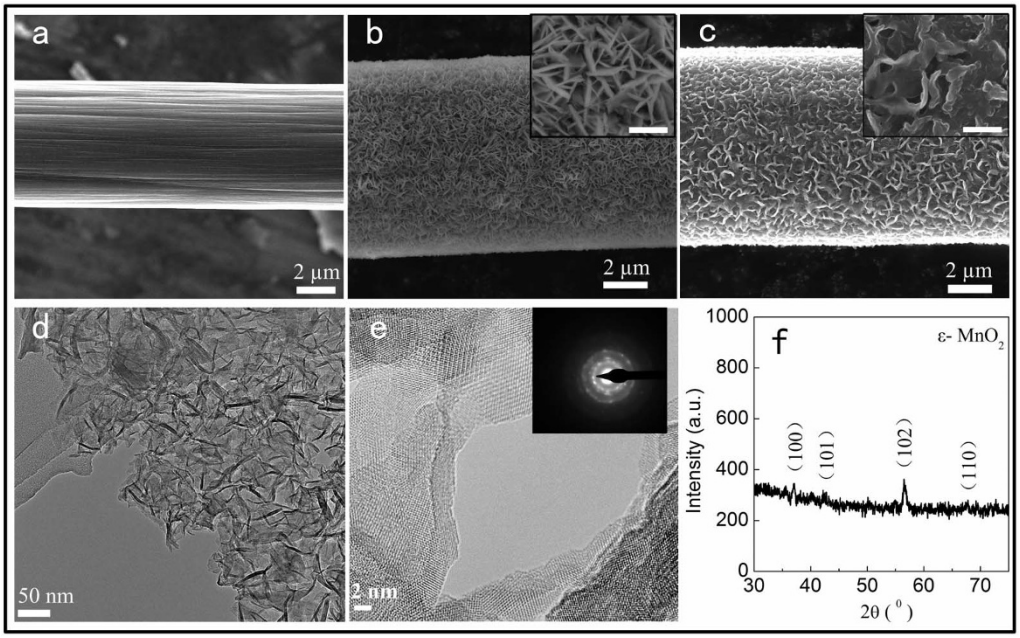

Figure 2 | Characterization of PPy-MnO_2-CF electrodes. (a) A SEM image of a CF; (b) MnO_2 nanoflakes uniformly deposited on the CF; (c) A SEM image of PPy wrapping on the MnO_2-CF, scale bars of the insets in (b) and (c): 1 μm; (d) A TEM image of MnO_2 nanoflakes; (e) High resolution TEM image and the inset SAED pattern of MnO_2 nanoflakes showing the polycrystalline nature of MnO_2; (f) XRD of MnO_2 structure showing the ε-MnO_2 phase.

2 min. When PPy was wrapped on MnO_2 nanoflakes, the porous and the space among the nanoflakes were fully or partly filled. So, PPy and ε-MnO_2 formed an organic-inorganic composite material and coated the CF. Therefore we expected a high performance SC.

Electrochemical characterizations of all solid-state SCs based on PPy-MnO_2 nanoflakes-CF hybrid structure. To evaluate the electrochemical performance of the PPy-MnO_2 nanoflakes-CFs hybrid structure, two-electrode configuration was used in the electrochemical measurements. As illustrated in Figure 3a, two cyclic voltammetry (CV) curves almost overlapped with each other. However, they came from different devices: one was from CFs SC, the other was from MnO_2- CFs SC. Figure 3b was a SEM image of a MnO_2 nanoflakes-CF, region I was immersed into H_3PO_4 solution of 9.1 wt. % for 12 h. The concentration of the H_3PO_4 was the same of the gel electrolyte of PVA/H_3PO_4. Region II was above the liquid surface. It was clear to see that MnO_2 nanoflakes on the CF had been eroded completely after immersing in H_3PO_4 solution for 12 h. This was the reason of the two CV curves overlapped in Figure 3a which indicated that MnO_2 nanoflakes was eroded and had no effects in improving the electrochemical performances of the device. Figure 3c was CV curves obtained from CFs SC, PPy-CFs SC and PPy-MnO_2-CFs SC at the same scan rate of 100 mV s^{-1}, respectively. The area of the CV curve of PPy-CFs SC was about 33 times larger than that of the CFs SC. It revealed that PPy had good electrochemical performances, which was consistent with the previous work[37]. When PPy coated on MnO_2 nanoflakes after an in situ growth process and was fabricated into a SC, the area of CV was much larger not only than that of the CFs SC, but also than that of the PPy-CFs SC (Figure 3c). Figure 3d is a SEM image of a PPy-MnO_2 nanoflakes-CF after being immersed into H_3PO_4 solution of the same concentration for 24 h. It demonstrated that PPy-MnO_2 nanoflakes had not been eroded by H_3PO_4, which is supported by the comparison between Figure 2c (as-prepared PPy-MnO_2-CF) and Figure 3d (PPy-MnO_2-CFs into H_3PO_4 solution), and resulted the perfect CV measurements showed in Figure 3c. Thus, we suggest that there are three reasons for the large enhancement of the electrochemical performances: First, PPy has also a good capacitance characteristics, and both PPy and MnO_2 play an important role in the electrochemical performances of the device. Second, PPy is an anti-corrosion material in the acidic PVA/H_3PO_4 electrolyte and protects MnO_2 nanoflakes against corrosion. Third, though MnO_2 has poor electronic and ionic conductivities, PPy can improve the conductivity of the electrode material largely after the "conductive wrapping" process.

In order to study the relationship between the electrodeposition time and the performances of the devices, there were two steps in the optimization process. At first, we adopted a constant time for PPy electrodeposition of 1 min, and the MnO_2 deposition time was from 1 to 45 min. CV curves corresponding to the different MnO_2 deposition time were measured as illustrated in Figure 4a, b. All the CV curves were at a scan rate of 10 mV s^{-1} but had obvious differences. Figure 4c showed the relationship of the specific capacitances and the MnO_2 deposition times. The optimal deposition time for MnO_2 was about 15 min. The second step was to gain the best deposition time of PPy after 15 min MnO_2 optimal deposition. We adopted a constant time for MnO_2 deposition of 15 min while the deposition time of PPy ranged from 0.5 to 3 min. CV curves were measured as shown in Figure 4d and e. The optimal electrodeposition time of PPy was about 2 min as illustrated in Figure 4f. Thus, we had obtained the optimal deposition time of 15 min and 2 min for MnO_2 and PPy, respectively. So we could fabricate all solid-state high performances SCs based on the optimization process.

In order to investigate the performances of the SC fabricated with the optimal electrodeposition process of the electrode materials, CV measurements were performed using two-electrode configurations. Figure 5a and b showed the CVs of the as-fabricated device at scan rates from 1 to 200 mV s^{-1} within a potential window of 0.8 V. The CV curves had large enclosed area and good symmetrical rectangular shape, showing that the capacitive behaviour of the device could be greatly improved by optimizing the electrodeposition time of MnO_2 and PPy. Galvanostatic charge-discharge (GCD) and electrochemical impedance spectroscopy (EIS) measurements were carried to further evaluate the electrochemical performances of the device.

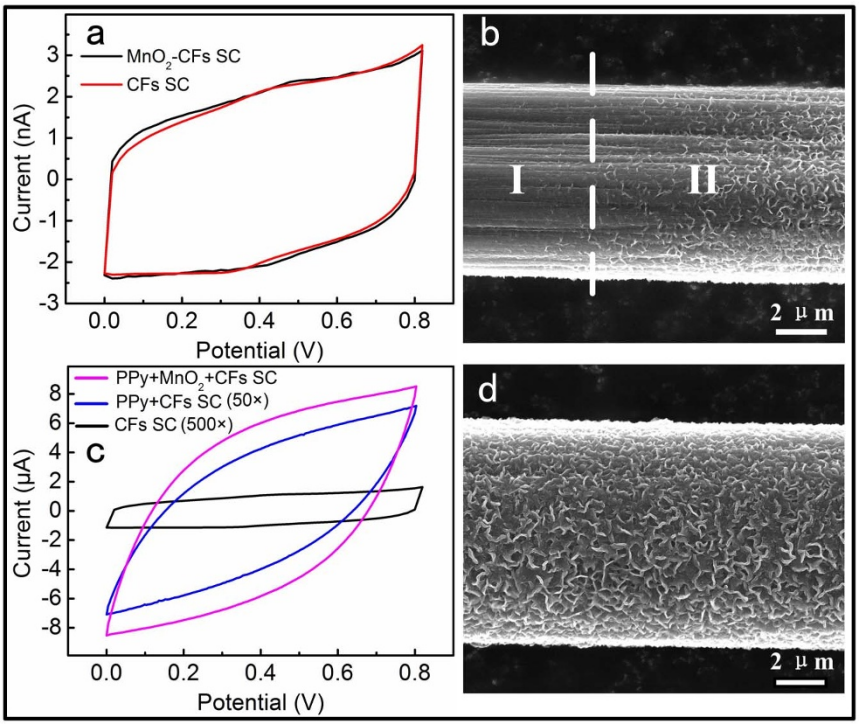

Figure 3 | Comparison of the different electrode materials. (a) CV curves of MnO_2-CFs SC and CFs SC. (b) A SEM image of a MnO_2-CF: region I was immersed into H_3PO_4 solution of 9.1 wt. % for 12 h; region II was above the liquid surface. (c) CV curves of PPy-MnO_2-CFs, PPy-CFs SC and CFs SC. For comparison, the current of CFs SC and PPy-CFs SC were magnified 500 and 50 times to their measuring value, respectively. (d) A SEM image of a PPy-MnO_2-CF after it was immersed into H_3PO_4 solution of 9.1 wt. % for 24 h. It remains the feature of the as-prepared PPy-MnO_2-CF (see figure 2c). The scan rate of all the CV curves was 100 mV s^{-1}.

The GCD curves at different current densities ranging from 0.1 to 1 A cm^{-3} were shown in Figure 5c, through which good linear potential-time profiles were achieved, demonstrating a good capacitance performance of the devices. The average diameter of the PPy-MnO_2-carbon fibers was about 9.5 μm. The fiber was considered as a cylinder when we estimated its volume. The highest volume capacitance is 69.3 F cm^{-3} at a current density of 0.1 A cm^{-3} which was much higher than those reported in literature[37,39,40], and remain

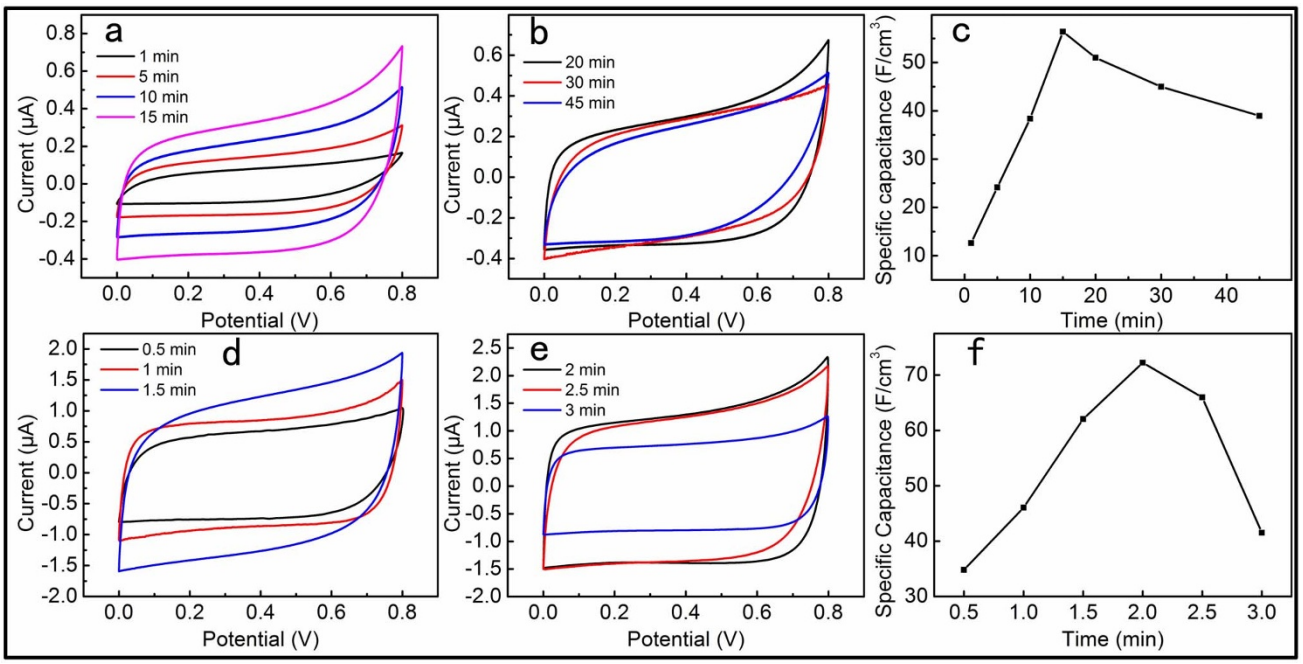

Figure 4 | Electrochemical behaviours of PPy-MnO_2-CFs SCs with different growth conditions of their electrode materials. (a and b) CV curves of the SCs with MnO_2 electrodeposition time from 1 to 45 min; (c) specific capacitances vs MnO_2 electrodeposition time; (d and e) CV curves of the SCs with PPy electrodeposition time from 0.5 to 3 min; (f) specific capacitances vs PPy electrodeposition time. The scan rate of all the CV curves was 10 mV s^{-1}.

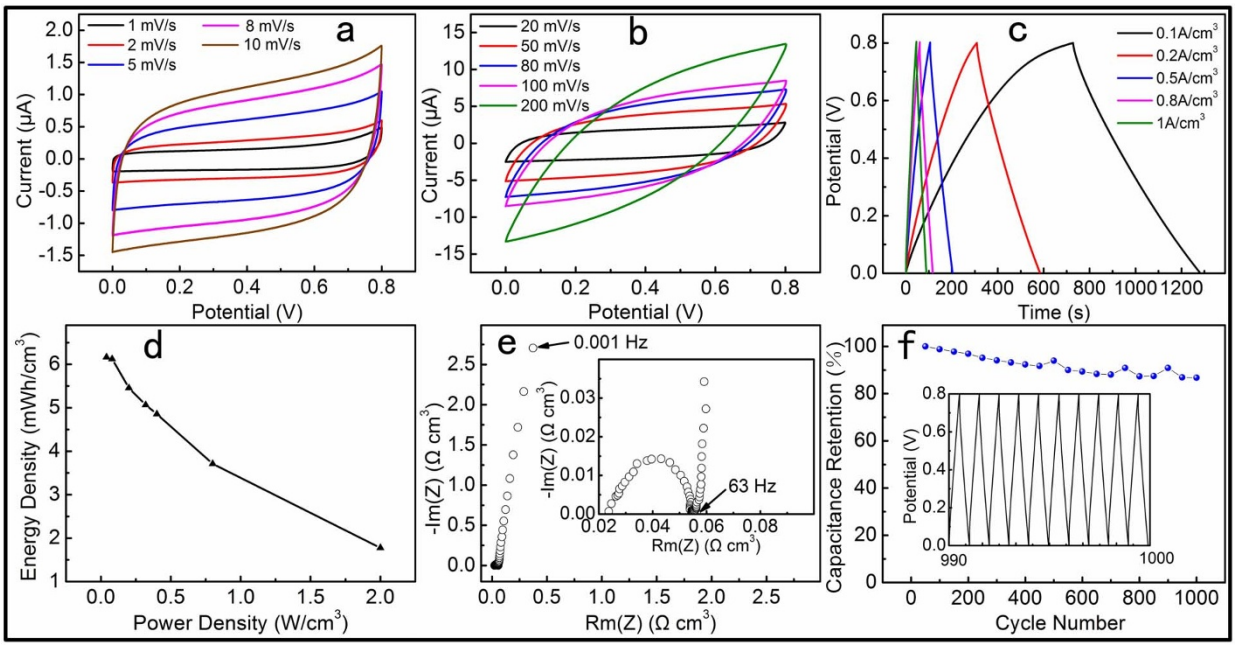

Figure 5 | Electrochemical performances of the PPy-MnO_2-CFs SC with 15 min MnO_2 deposition and 2 min PPy deposition. (a and b) CV curves of the device at scan rates from 1 to 200 mV s^{-1}; (c) GCD curves of the device under different current densities; (d) energy and power density plot; (e) Nyquist plot; (f) Cycle life, the inset is the GCD curve from the 990th to 1000th cycle.

at 54.6 F cm^{-3} at 1 A cm^{-3}, revealing the good rate capability of the device. Figure 5d is the Rogone plot, showing the energy density with respect to the average power density of the as-fabricated all-solid-state SC. The power density of the device achieved 0.4 W cm^{-3} while the energy density was still at 4.86 mW h cm^{-3}. Since EIS and long-term cycling stability are two important parameters for practical applications of the SC. Figure 5e and inset showed the Nyquist plot in the frequency range from 0.001 Hz to 100 KHz. The straight line is nearly parallel to the imaginary axis, revealing an ideal capacitive behaviour of the device. The knee frequency f_0 of the SC is about 63 Hz and its relaxation time constant τ_0 is about 16 ms ($\tau_0 = 1/f_0$). The long-term cycle stability was measured by GCD at a current density of 1 A cm^{-3} for 1000 cycles and the result is shown in Figure 5f. The capacitance of the SC decreased gradually during the whole process besides several slight fluctuations in some cycles. The capacitance retention was about 86.7% after cycling for 1000 times. It is a very good cycling performance among the reported works for PPy-based SCs[41–44].

For the consideration of application in practice, portable and flexible electronics may require highly flexible power sources working at different operation voltages and powers. An all-solid-state SC was assembled by two PPy-MnO_2 nanoflakes-CF hybrid electrodes on a piece of common preservative film. The as-fabricated SC is lightweight and highly flexible, which can be twisted and rolled up without destroying the structural integrity of the device, as can be seen in Figure 6a and b. The CV curves in Figure 6c almost overlap completely. The CV areas at the same scan rate of 10 mV s^{-1} are 2.086 and 2.091 when the device was unfolded and rolled up, respectively. There is only a slight fluctuation of about 0.24% in the electrochemical performances of the SC. In addition, the rectangular profile of CV curves indicated the ideal pseudocapacitive nature of PPy-MnO_2 nanoflakes and fast redox reaction with solid electrolyte of H_3PO_4/PVA. When it is need to provide different voltages or currents, SCs would be connected in series or in parallel. Figure 6d shows a schematic of three SCs connected in series. The test results are showed in Figure 6f. The calculated capacitances of device 1 and 2 are 0.24 and 0.22 mF, respectively. When they have been connected in series, the capacitance of the whole device is calculated to be 0.11 mF, when in parallel, it is 0.48 mF. The results reveal that the capacitance of the whole device roughly obeys the basic rule of series and parallel connections of capacitors when the SC has been connected with others. So we can take various connections of SCs to meet the demand in practice. An example for the application of the connected SCs is showed in Figure 6e and the inset in Figure 6f, where three SCs are connected in series, and can drive a commercial LCD as an energy source when it has been full charged.

Discussion

The above obtained excellent electrochemical performances of the as-fabricated solid-state SCs are not simply a result of the mixture of the two active materials (PPy & MnO_2). It is suggested that these performance advancements may originate from the efficient integration of each advantages from both PPy and MnO_2 in the whole device. The rational design with the worthwhile merits achieved by coating conductive PPy on high-capacitance MnO_2 nanoflakes provides several unique features: (i) MnO_2 nanoflakes have lager specific area, which is conducive to the electrochemical performance of the device, both PPy and MnO_2 play important roles in the electrochemical performances of the device; (ii) PPy is an anti-corrosion material in the acidic PVA/H_3PO_4 electrolyte and protected MnO_2 nanoflakes against corrosion, which ensure full play of high specific capacitance of MnO_2; (iii) though MnO_2 has poor electronic and ionic conductivities, but the conductivities of PPy are good. The uniform conductive coating of PPy membrane provided another transmission path for charges and ions, and potentially offer better interconnectivity within MnO_2 nanoflakes which improve the conductivity of the electrode material largely. Since it has simple, rapid and uniform coated features, our "in situ growth of conductive wrapping" method is an efficient way to design and fabricate high performance SCs based on organic-inorganic composite nanostructures.

In summary, we have successfully fabricated a solid-state SC based on a PPy-MnO_2 nanoflakes-CF hybrid structure by an "in situ growth for conductive wrapping" method. The device exhibited high electrochemical performances, such as a high volume capacitance of 69.3 F cm^{-3} at a discharge current density of 0.1 A cm^{-3}, a high energy density of 6.16 $\times$ 10^{-3} Wh cm^{-3} at a power density of

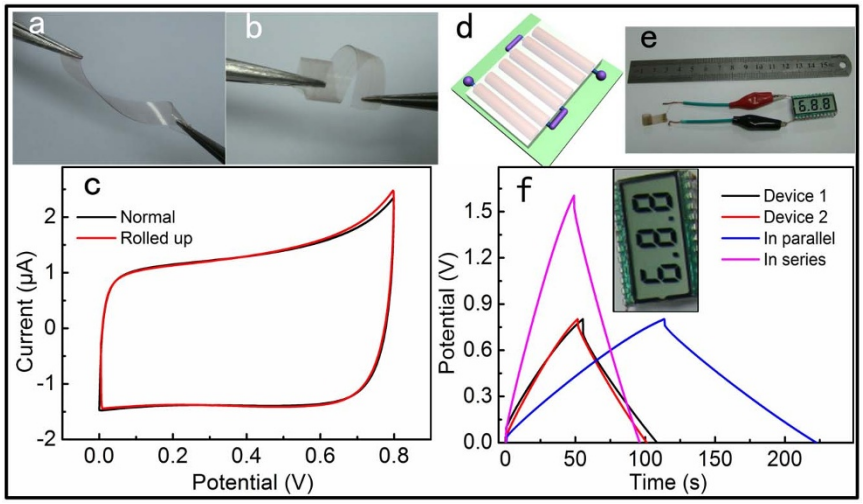

Figure 6 | Optical images of twisted (a) and bended SCs (b). (c) CV curves of normal and rolled SCs. (d) The schematic of the three SCs connected in series. (e) Optical image of the three SCs in series drove a LCD. (f) GCD curves of single SC and two SCs connected in series or in parallel. The inset was a partial enlarged view of Figure 6e.

0.04 W cm^{-3}, and good cycling stability. Our experiment confirmed that the PPy protect MnO_2 nanoflakes against the corrision of acid electrolyte, which enhances the electrochemical performances significantly. In addition, the as-fabricated solid-state SC showed high mechanical flexibility, and the capacitance of the device had only a slight fluctuation of 0.24% when it was rolled up. The good performances of the device indicated that organic-inorganic composite materials might have certain advantages than one component as the active electrode materials in SCs, and the "in situ growth of conductive wrapping" method would have enormous potential applications in the design of high-performance SCs. The successful attempt to drive a commercial LCD shows that our device has the opportunity to be applied in energy storage and flexible/portable electronics.

Methods

Fabrication of electrodes and SCs. CFs with a diameter about 8 μm were used as the charge collector. MnO_2 nanoflakes were grown on the CF via a electrochemical deposition process using a solution of 20 mM $Mn(NO_3)_2$ and 100 mM $NaNO_3$[45]. Three-electrode configuration was used in the deposition process with Ag/AgCl as reference electrode, platinum foil as counter electrode, and the CF as working electrode. A constant voltage of 0.92 V was required during the process. Then the MnO_2-CF was washed in deionized water and dried at room temperature. PPy was deposited using a similar method and formed a conductive wrapping on the MnO_2-CF, using a solution of 0.2 M $NaClO_4$ and 5% (V : V) pyrrole monomer.

The gel electrolyte was prepared by adding 6 g of H_3PO_4 and 6 g of polyvinyl alcohol (PVA) powder into 60 ml of deionized water. The mixture was heated to 85°C with stirring until the solution became clear. Two PPy-MnO_2-CFs were located on a piece of preservative film closely and in parallel. The separation space was about 1 mm. Then the whole device was immersed into the PVA/H_3PO_4 electrolyte for 5 minutes. After that, the device was put into fume hood at room temperature to vaporize the excess water. When the gel electrolyte solidified, the two electrodes were packaged and the SC was prepared.

Characterization. The morphologies, structure, and chemical composition of the samples were characterized by high-resolution field emission scanning electron microscopy (FEI Nova Nano-SEM 450), Probe Cs-corrected transmission electron microscopy (FEI Titan G^2 60–300), and XRD (PANalyticalB.V.X'PertPRO). All the electrochemical measurements were carried out in a two-electrode system at room temperature using Autolab PGSTAT302N (Metrohm AG). The electrochemical impedance spectroscopy was measured ranging from 1 mHz to 100 KHz with a potential amplitude of 10 mV. The mechanical flexibility test was carried out by manual control, where the whole device was rolled up by hand.

1. Rogers, J. A. & Huang, Y. G. A curvy, stretchy future for electronics. *P. Natl. Acad. Sci. USA* **106**, 10875–10876 (2009).
2. Kim, D. H. *et al.* Epidermal Electronics. *Science* **333**, 838–843 (2011).
3. Someya, T. *et al.* Conformable, flexible, large-area networks of pressure and thermal sensors with organic transistor active matrixes. *P. Natl. Acad. Sci. USA* **102**, 12321–12325 (2005).
4. Lipomi, D. J. *et al.* Skin-like pressure and strain sensors based on transparent elastic films of carbon nanotubes. *Nat. Nanotechnol.* **6**, 788–792 (2011).
5. Whittingham, M. S. Materials challenges facing electrical energy storage. *Mrs Bull.* **33**, 411–419 (2008).
6. Simon, P. & Gogotsi, Y. Materials for electrochemical capacitors. *Nat. Mater.* **7**, 845–854 (2008).
7. Hall, P. J. *et al.* Energy storage in electrochemical capacitors: designing functional materials to improve performance. *Energ. Environ. Sci.* **3**, 1238–1251 (2010).
8. Brezesinski, T., Wang, J., Tolbert, S. H. & Dunn, B. Ordered mesoporous alpha-MoO_3 with iso-oriented nanocrystalline walls for thin-film pseudocapacitors. *Nat. Mater.* **9**, 146–151 (2010).
9. Song, M. K. *et al.* Anomalous Pseudocapacitive Behavior of a Nanostructured, Mixed-Valent Manganese Oxide Film for Electrical Energy Storage. *Nano Lett.* **12**, 3483–3490 (2012).
10. Zhang, L. L. & Zhao, X. S. Carbon-based materials as supercapacitor electrodes. *Chem. Soc. Rev.* **38**, 2520–2531 (2009).
11. Arico, A. S., Bruce, P., Scrosati, B., Tarascon, J. M. & Van Schalkwijk, W. Nanostructured materials for advanced energy conversion and storage devices. *Nat. Mater.* **4**, 366–377 (2005).
12. Meng, C. Z., Liu, C. H., Chen, L. Z., Hu, C. H. & Fan, S. S. Highly Flexible and All-Solid-State Paper like Polymer Supercapacitors. *Nano Lett.* **10**, 4025–4031 (2010).
13. Kaempgen, M., Chan, C. K., Ma, J., Cui, Y. & Gruner, G. Printable Thin Film Supercapacitors Using Single-Walled Carbon Nanotubes. *Nano Lett.* **9**, 1872–1876 (2009).
14. Weng, Z. *et al.* Graphene-Cellulose Paper Flexible Supercapacitors. *Adv. Energy Mater.* **1**, 917–922 (2011).
15. Yuan, L. Y. *et al.* Flexible Solid-State Supercapacitors Based on Carbon Nanoparticles/MnO_2 Nanorods Hybrid Structure. *Acs Nano* **6**, 656–661 (2012).
16. Xiao, X. *et al.* WO_{3-x}/MoO_{3-x} Core/Shell Nanowires on Carbon Fabric as an Anode for All-Solid-State Asymmetric Supercapacitors. *Adv. Energy Mater.* **2**, 1328–1332 (2012).
17. Li, Q. *et al.* Design and Synthesis of MnO_2/Mn/MnO_2 Sandwich-Structured Nanotube Arrays with High Supercapacitive Performance for Electrochemical Energy Storage. *Nano Lett.* **12**, 3803–3807 (2012).
18. Liu, J. P. *et al.* Co_3O_4 Nanowire@MnO2 Ultrathin Nanosheet Core/Shell Arrays: A New Class of High-Performance Pseudocapacitive Materials. *Adv. Mater.* **23**, 2076–2081 (2011).
19. Lu, X. H. *et al.* Hydrogenated TiO_2 Nanotube Arrays for Supercapacitors. *Nano Lett.* **12**, 1690–1696 (2012).
20. Guan, C. *et al.* Hybrid structure of cobalt monoxide nanowire@nickel hydroxidenitrate nanoflake aligned on nickel foam for high-rate supercapacitor. *Energ. Environ. Sci.* **4**, 4496–4499 (2011).
21. Guan, C. *et al.* Nanoporous Walls on Macroporous Foam: Rational Design of Electrodes to Push Areal Pseudocapacitance. *Adv. Mater.* **24**, 4186–4190 (2012).
22. Toupin, M., Brousse, T. & Belanger, D. Charge storage mechanism of MnO_2 electrode used in aqueous electrochemical capacitor. *Chem. Mater.* **16**, 3184–3190 (2004).
23. Fischer, A. E., Pettigrew, K. A., Rolison, D. R., Stroud, R. M. & Long, J. W. Incorporation of homogeneous, nanoscale MnO_2 within ultraporous carbon

structures via self-limiting electroless deposition: Implications for electrochemical capacitors. *Nano Lett.* **7**, 281–286 (2007).
24. Yu, G. H. *et al.* Solution-Processed Graphene/MnO_2 Nanostructured Textiles for High-Performance Electrochemical Capacitors. *Nano Lett.* **11**, 2905–2911 (2011).
25. Hu, L. B. *et al.* Symmetrical MnO_2-Carbon Nanotube-Textile Nanostructures for Wearable Pseudocapacitors with High Mass Loading. *Acs Nano* **5**, 8904–8913 (2011).
26. Lang, X. Y., Hirata, A., Fujita, T. & Chen, M. W. Nanoporous metal/oxide hybrid electrodes for electrochemical supercapacitors. *Nat. Nanotechnol.* **6**, 232–236 (2011).
27. Ma, S. B. *et al.* Electrochemical properties of manganese oxide coated onto carbon nanotubes for energy-storage applications. *J. Power Sources* **178**, 483–489 (2008).
28. Sivakkumar, S. R., Ko, J. M., Kim, D. Y., Kim, B. C. & Wallace, G. G. Performance evaluation of CNT/polypyrrole/MnO2 composite electrodes for electrochemical capacitors. *Electrochi. Acta* **52**, 7377–7385 (2007).
29. Lee, S. W., Kim, J., Chen, S., Hammond, P. T. & Shao-Horn, Y. Carbon Nanotube/Manganese Oxide Ultrathin Film Electrodes for Electrochemical Capacitors. *Acs Nano* **4**, 3889–3896 (2010).
30. Hu, L. B. *et al.* Stretchable, Porous, and Conductive Energy Textiles. *Nano Lett.* **10**, 708–714 (2010).
31. Yan, J. *et al.* Fast and reversible surface redox reaction of graphene-MnO_2 composites as supercapacitor electrodes. *Carbon* **48**, 3825–3833 (2010).
32. Liu, R. & Lee, S. B. MnO_2/Poly(3,4-ethylenedioxythiophene) coaxial nanowires by one-step coelectrodeposition for electrochemical energy storage. *J. Am. Chem. Soc.* **130**, 2942–2943 (2008).
33. Chen, L. *et al.* Synthesis and pseudocapacitive studies of composite films of polyaniline and manganese oxide nanoparticles. *J. Power Sources* **195**, 3742–3747 (2010).
34. Yu, G. H. *et al.* Enhancing the Supercapacitor Performance of Graphene/MnO_2 Nanostructured Electrodes by Conductive Wrapping. *Nano Lett.* **11**, 4438–4442 (2011).
35. Wang, D. *et al.* Spontaneous Growth of Free-Standing Polypyrrole Films at an Air/Ionic Liquid Interface. *Langmuir* **26**, 14405–14408 (2010).
36. Song, K. T. *et al.* Solvent effects on the characteristics of soluble polypyrrole. *Synthetic Met.* **110**, 57–63 (2000).
37. Yuan, L. Y. *et al.* Polypyrrole-coated paper for flexible solid-state energy storage. *Energ. Environ. Sci.* **6**, 470–476 (2013).
38. Davoglio, R. A., Biaggio, S. R., Bocchi, N. & Rocha, R. C. Flexible and high surface area composites of carbon fiber, polypyrrole, and poly(DMcT) for supercapacitor electrodes. *Electrochi. Acta* **93**, 93–100 (2013).
39. Lu, X. H. *et al.* Stabilized TiN Nanowire Arrays for High-Performance and Flexible Supercapacitors. *Nano Lett.* **12**, 5376–5381 (2012).
40. Xiao, X. *et al.* Fiber-Based All-Solid-State Flexible Supercapacitors for Self-Powered Systems. *Acs Nano* **6**, 9200–9206 (2012).
41. Nystrom, G., Razaq, A., Stromme, M., Nyholm, L. & Mihranyan, A. Ultrafast All-Polymer Paper-Based Batteries. *Nano Lett.* **9**, 3635–3639 (2009).
42. Razaq, A., Nyholm, L., Sjodin, M., Stromme, M. & Mihranyan, A. Paper-Based Energy-Storage Devices Comprising Carbon Fiber-Reinforced Polypyrrole-Cladophora Nanocellulose Composite Electrodes. *Adv. Energy Mater.* **2**, 445–454 (2012).
43. Olsson, H., Nystrom, G., Stromme, M., Sjodin, M. & Nyholm, L. Cycling stability and self-protective properties of a paper-based polypyrrole energy storage device. *Electrochem. Commun.* **13**, 869–871 (2011).
44. Khomenko, V., Raymundo-Pinero, E., Frackowiak, E. & Beguin, F. High-voltage asymmetric supercapacitors operating in aqueous electrolyte. *Applied Physics A-Mater.* **82**, 567–573 (2006).
45. Chen, W. *et al.* High-Performance Nanostructured Supercapacitors on a Sponge. *Nano Lett.* **11**, 5165–5172 (2011).

Acknowledgements

This work was supported by the National Basic Research Program (2011CB933300) of China, the National Natural Science Foundation of China (11204093, 11074082), and the Fundamental Research Funds for the Central Universities (HUST: 2012QN114, 2013TS033).

Author contributions

N.S.L. & Y.H.G. devised the original concept, designed the experiments, discussed the interpretation of results and revised the paper; J.Y.T. & W.Z.M. performed the experiments with equal contribution; J.Y.T. wrote the draft of the manuscript; L.W.D., L.Y.L. & J.S. contributed the TEM microstructure experiment. All authors discussed the results and participated in manuscript revision.

Additional information

Supplementary information accompanies this paper at http://www.nature.com/scientificreports

Competing financial interests: The authors declare no competing financial interests.

How to cite this article: Tao, J. *et al.* Solid-State High Performance Flexible Supercapacitors Based on Polypyrrole-MnO_2-Carbon Fiber Hybrid Structure. *Sci. Rep.* **3**, 2286; DOI:10.1038/srep02286 (2013).